Title
Multiexciton Lifetimes Reveal Triexciton Emission Pathway in CdSe Nanocrystals.

Journal
Nano letters, 18(8)

ISSN
1530-6984

Authors
Shulenberger, Katherine E
Bischof, Thomas S
Caram, Justin R
et al.

Publication Date
2018-08-01

DOI
10.1021/acs.nanolett.8b02080

Peer reviewed

NANO LETTERS
Letter
Cite This: Nano Lett. 2018, 18, 5153−5158
pubs.acs.org/NanoLett

Multiexciton Lifetimes Reveal Triexciton Emission Pathway in CdSe Nanocrystals

Katherine E. Shulenberger,[‡] Thomas S. Bischof,[‡] Justin R. Caram,[†] Hendrik Utzat, Igor Coropceanu, Lea Nienhaus, and Moungi G. Bawendi*

Department of Chemistry, Massachusetts Institute of Technology, 77 Massachusetts Avenue, Cambridge, Massachusetts 02139, United States

Supporting Information

ABSTRACT: Multiexcitons in emerging semiconducting nanomaterials play a critical role in potential optoelectronic and quantum computational devices. We describe photon resolved single molecule methods to directly probe the dynamics of biexcitons and triexcitons in colloidal CdSe quantum dots. We confirm that biexcitons emit from a spin-correlated state, consistent with statistical scaling. Contrary to current understanding, we find that triexciton emission is dominated by band-edge $1S_e1S_{3/2}$ recombination rather than the higher energy $1P_e1P_{3/2}$ recombination.

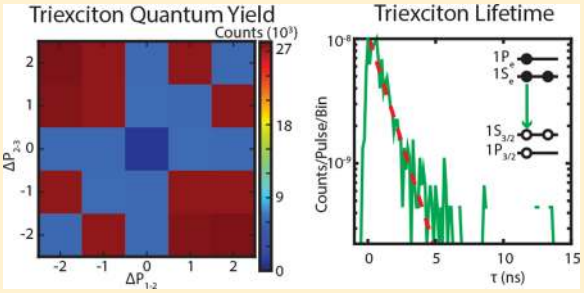

KEYWORDS: *Semiconductor nanocrystal, biexciton, triexciton, Auger recombination, single molecule spectroscopy, photon correlation*

Nanocrystals (NCs) are of interest as fluorophores for lasing and display technologies[1−5] and single-photon sources for quantum computing applications[6] due to emission wavelength tunability from the ultraviolet to the infrared via particle size and material composition,[7] high single-exciton photo luminescence (PL) quantum yield, and relatively narrow emission line width.[8] To facilitate improvements in NC device functionality and expand NC applications, it is crucial to understand how competing radiative and nonradiative processes contribute to observed NC multiexciton emission dynamics and quantum yield.

Recent years have shown a breakthrough in understanding how to control Auger recombination rates in colloidal NCs and therefore biexciton quantum yields.[9−14] Multiexciton emission is primarily quenched by Auger recombination when an exciton recombines and excites a third carrier to a higher energy state, dissipating energy without emitting a photon.[15] Experimental and theoretical studies of core/shell samples of II−VI CdSe based NCs suggest that the core/shell interface is crucial in determining the rate of Auger recombination, which has led to the synthesis of NC samples with unity biexciton (BX) quantum yield.[9,12,13] It has generally been assumed that BX emission from II−VI and III−V NCs originates from two spin-correlated, band-edge excitons, yielding a four-times faster radiative rate for the BX in confined, zero-dimensional NCs as compared to the single exciton (X) radiative rate.[12,16−18]

Higher-order multiexcitons (≥3) in CdSe NCs occupy not just the S-like ($1S_e1S_{3/2}$) band-edge states, but the higher-lying, P-like ($1P_e1P_{3/2}$) states as well.[19−22] Current methods to interrogate the triexciton (TX) rely on modeling of flux-dependent ensemble PL lifetimes, spectrally filtering emission after high-flux excitation, or low temperature (∼4 K) measurements where multiexciton emission is spectrally distinct.[19−21,23] Results from these studies demonstrate that if emission from the P-like state occurs, it precedes S-like emission.[21] Additionally, S-like triexciton recombination was measured to have a larger yield than P-like recombination at low temperature in CdTe/CdSe NCs, which are analogous to CdSe/CdS. However, none of these studies were able to identify the dominant emissive state for the CdSe triexciton at room temperature, and many works continue to assume triexciton recombination occurs from the P-like state.[18,24,25]

In this work, using CdSe based NCs, we extend single photon methods to resolve the dynamics of individual multiexcitonic states. We unambiguously measure the factor of 4 rate increase for the BX radiative rate as compared to the X as a demonstration of the power of this technique. We then utilize this method to conclusively identify the origin of TX emission, which had not been possible with previous state-of-the art methods. Finally, we are able to extract all Auger rates and determine that band-edge processes dominate the yield of both BX and TX recombination.

We designed a fluorescence microscope and an analysis algorithm to optimize for multiexciton dynamics detection, utilizing number-resolved, time-correlated single photon counting spectroscopy of individual NCs. The microscope is schematically illustrated in Figure 1a. We collect the fluorescence from a single NC isolated on a glass substrate in a dilute film (<0.1 NC/μm^2) excited by a pulsed excitation source. The emitted photon stream is spatially filtered with a

Received: May 22, 2018
Revised: June 24, 2018
Published: July 17, 2018

DOI: 10.1021/acs.nanolett.8b02080
Nano Lett. 2018, 18, 5153−5158

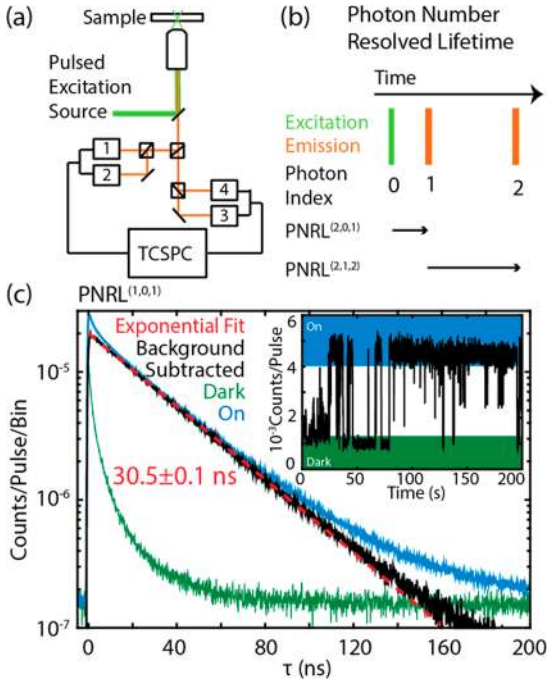

Figure 1. (a) Schematic of the home-built fluorescence microscope used to collect data containing four single photon counting modules. (b) Definitions of PNRL histograms. (c) Fluorescence lifetimes of intensity states as defined in the inset. The red dotted line is an exponential fit to the background subtracted fluorescence lifetime.

50 μm pinhole and then split equally between four single photon counting modules. For BX studies, we select a power such that the three-photon absorption rate is less than 1% of the two-photon absorption rate. We leverage the Poissonian absorption statistics of the NC to separate the number of absorbed Xs, BXs, and TXs by multiple orders of magnitude. Therefore, when sorting emission by the number of photons detected after a single excitation pulse, we ensure that a two photon detection event necessarily corresponds to a biexciton.

We resolve the dynamics of the BX and TX states through the photon number resolved lifetime (PNRL) algorithm, illustrated in Figure 1b and previously described by Canneson et al.[26] and Bischof et al.[11] For number resolution to accurately reflect the dynamics of the desired state, it is crucial to excite samples at sufficiently low fluxes that the Poissonian absorption properties of the NC ensure higher order multiexcitons are at least two orders of magnitude less likely. For example, when extracting BX dynamics and quantum yield, TX formation events must be one hundred times less likely. To obtain PNRLs we sort the emitted photon stream by the number of photons detected per pulse. We then histogram the arrival time of each photon relative to the prior photon index. We modify the notation introduced by Bischof et al.[11] to $\mathrm{PNRL}^{(\mathbf{x},\mathbf{y},\mathbf{z})}$ such that the superscript **x** represents the number of photons detected per excitation pulse, **y** is the start index, and **z** is the stop index.

The samples studied here consist of core/shell spherical CdSe NCs. Unless otherwise specified, samples are core/shell CdSe NCs obtained from QDVision. Shell thickness studies were performed on a series of CdSe/CdS NCs with 1 to ~8 monolayers of CdS synthesized according to ref 27.

When operating at low-flux, NC emission is only ~5 times as intense as background emission. Therefore, we must thoroughly characterize and subtract the background dynamics to isolate NC signal. To do so, we exploit the binary blinking of NCs (Figure 1c inset). In Figure 1c, we plot the PL lifetime of both the "on" (blue) and "dark" (green) states determined from the fluorescence intensity trace. The dynamics of the dark state, plotted in Figure S2, are dominated by emission from the substrate, verifying that the origin of the dark emission is predominantly unrelated to the NC. To obtain the intrinsic NC lifetime we subtract the "dark" emission dynamics from the on-state dynamics, effectively isolating NC emission. This leads to a monoexponential decay for exciton emission (Figure 1c, black). We fit the PL decay to a single exponential and obtain a radiative lifetime of 30.5 ± 0.1 ns, which is consistent with previously reported values for similar NCs.[28,29]

To establish the effect of multiexciton interactions on the radiative recombination rate, we utilize the PNRL algorithm to measure the lifetime of the BX and compare that to the X dynamics.

$$r_{\mathrm{BX/X}} = \frac{k_{\mathrm{rad,BX}}}{k_{\mathrm{rad,X}}} = \frac{\tau_{\mathrm{X}}/QY_{\mathrm{X}}}{\tau_{\mathrm{BX}}/QY_{\mathrm{BX}}} \tag{1}$$

where $r_{\mathrm{BX/X}}$ is the scaling factor between the X and BX radiative rates, $k_{\mathrm{rad,BX}}$ is the BX radiative rate, $k_{\mathrm{rad,X}}$ is the X radiative rate, τ_{X} is the X lifetime (Figure 1c, black), $\mathrm{QY_{BX}}/\mathrm{QY_X}$ is the BX to X quantum yield ratio (Figure 2a, inset), and τ_{BX} is the BX lifetime. All of these values can be determined through our low-flux photon counting techniques.

Due to the low fraction of BX emission events, the BX lifetime is particularly sensitive to systematic error due to two-photon events with one photon originating from a background source. By convoluting the lifetime of the X and the background, we can calculate the background signal for two-photon dynamics.

$$\mathrm{PNRL}_{\mathrm{bkg}}^{(2,0,1)}(\tau) = \mathrm{PNRL}_{\mathrm{off}}^{(1,0,1)}(\tau)\int_{\tau}^{t_{\mathrm{rep}}} \mathrm{PNRL}_{\mathrm{NC}}^{(1,0,1)}(t)\,\mathrm{d}t + \mathrm{PNRL}_{\mathrm{NC}}^{(1,0,1)}(\tau)\int_{\tau}^{t_{\mathrm{rep}}} \mathrm{PNRL}_{\mathrm{off}}^{(1,0,1)}(t)\,\mathrm{d}t \tag{2}$$

where $\mathrm{PNRL}_{\mathrm{bkg}}^{(2,0,1)}$ is the two-photon event background signal, t_{rep} is the laser repetition rate, $\mathrm{PNRL}_{\mathrm{off}}^{(1,0,1)}$ is the lifetime of the dark state (Figure 1c, green), and $\mathrm{PNRL}_{\mathrm{NC}}^{(1,0,1)}$ is the NC X lifetime (Figure 1c, black). We subtract the dynamics calculated using eq 2 from the total $\mathrm{PNRL}^{(2,0,1)}$ signal to obtain the true BX dynamics (Figure S3). A thorough description of our background characterization methodologies can be found in the Supporting Information (SI). Additionally, since NC and coverslip emission are uncorrelated, the background emission described by eq 2 contributes equally to the center and side peaks in a $g^{(2)}$ correlation measurement as well and must be subtracted to extract the BX quantum yield. Failure to do so artificially increases the calculated BX yield (Figure S4). Here, we measure a value of 14.5 ± 0.3% for the background subtracted BX to X quantum yield ratio ($\mathrm{QY_{BX}}/\mathrm{QY_X}$).

We extract $r_{\mathrm{BX/X}}$ = 4.0 ± 0.1 from eq 1 using the measured BX to X quantum yield ratio (14.5%), the X lifetime (30.5 ns), and the measured BX lifetime of 1.1 ± 0.1 ns (Figure 2a). This result is consistent with statistical scaling of the state illustrated in Figure 2c,[18] which predicts a factor of 4 increase in rate for the BX relative to the X. At room temperature, only half of the X's are available to radiatively recombine due to spin selection

DOI: 10.1021/acs.nanolett.8b02080
Nano Lett. 2018, 18, 5153−5158

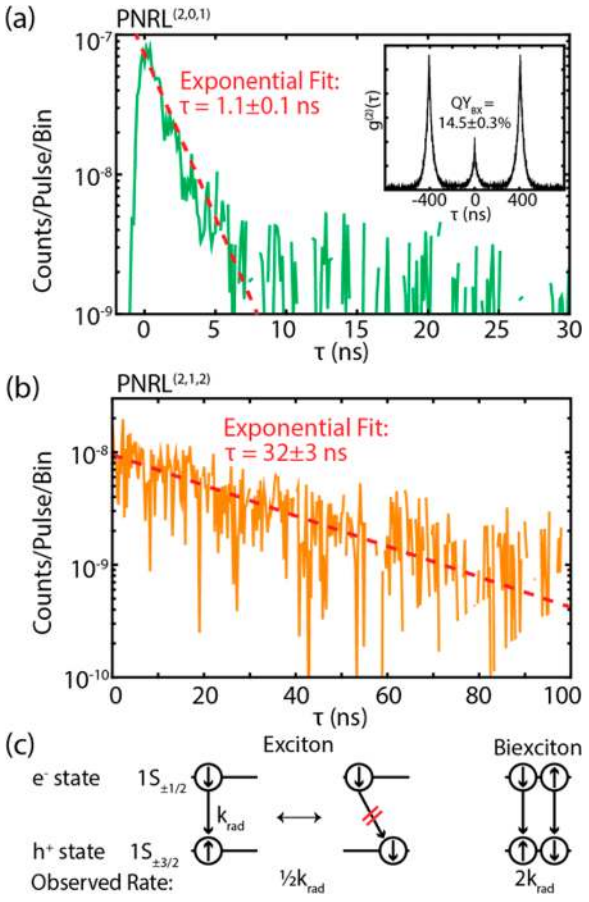

Figure 2. (a) Background subtracted biexciton lifetime (green). Data is fit to a single exponential (red). Inset is the second order correlation ($g^{(2)}$) for the same experiment. (b) Lifetime of the second photon emitted from a biexciton. Fit (red) is a single exponential. (c) Illustration of the origin of the difference in radiative rates for an exciton and bound biexciton in CdSe NCs.

rules. This is due to (1) the hole can rapidly spin mix (<10 ps), much faster than the radiative recombination time,[30−32] and (2) the spin-allowed and spin-forbidden states are only split by ∼1−5 meV, well within k_BT at room temperature. This leads to equal populations of the two states (±2 (dark), ± 1^L (bright)), with fast phonon-mediated exchange between them.[31,33] For the bound BX manifold, there are two spin-paired X's that can recombine independently, giving rise to a radiative speed up by a factor of 2 compared to a single spin-paired X. The combination of the factors of 1/2 (for the X) and 2 (for the BX) results in a BX radiative rate four times faster than that for the X.[11,16−18]

Next, we address the lifetime of the subsequent photon after BX recombination. In Figure 2b we plot the delay between the first and second photon of a BX ($PNRL^{(2,1,2)}$). For this NC, we measure a $PNRL^{(2,1,2)}$ value of 32 ± 3 ns, which is consistent with the X lifetime of 30.5 ± 0.1 ns. The agreement between these lifetimes indicates the X has no memory of the multiexciton state from which it originated. The lack of memory confirms that, in the absence of NC charging, all losses in device efficiency under high-flux excitation originate from low MX QY, rather than any change to the exciton emission pathway, and therefore, the best way to improve device performance is the reduction of Auger rates.

Having shown that BX emission in core/shell CdSe is consistent with the bound BX model illustrated in Figure 2c and that the remaining X has no memory, we now expand our studies to a shell-series. CdSe/CdS is a quasi-type II heterostructure where the electron delocalizes into the shell and the hole remains confined to the core, decreasing the electron−hole wave function overlap and increasing the X lifetime.[10] Increasing shell thickness also reduces the exchange energy, therefore decreasing the fine-structure splitting.[34] Figure 3a plots the measured BX lifetime against the product of τ_X and QY_{BX}. Using a linear fit, we extract $r_{BX/X}$ from the slope (eq 1).

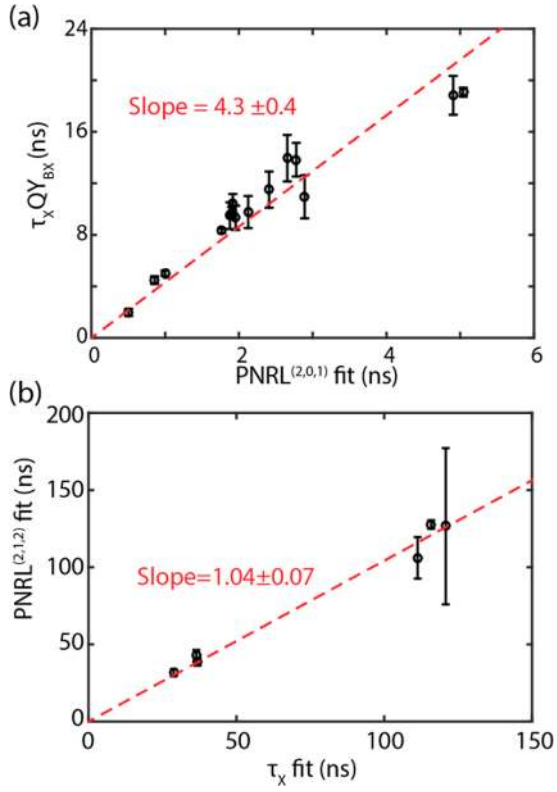

Figure 3. (a) Comparison of the biexciton lifetime and the product of the exciton lifetime and biexciton quantum yield. The data is fit to an error weighted first order polynomial (red). (b) Comparison of $PNRL^{(2,1,2)}$ and the exciton lifetime with an error weighted linear fit (red).

We obtain a slope of 4.3 ± 0.4 from an error weighted fit to a first-order polynomial with the intercept set to the origin. This result indicates universal agreement between BX emission and the bound BX model for shell thicknesses studied here. Figure 3b plots the X lifetime against the lifetime of the second photon of a BX. Error weighted fitting to a first-order polynomial with the intercept set to the origin gives a slope of 1.04 ± 0.07. The equivalence between the two lifetimes across all shell thicknesses confirms that previously reported rapid spin mixing is sufficient to ensure subsequent X emission has no observable memory of its origin in these NCs.[30,31]

We next utilize our ability to determine state specific quantum yields and dynamics to probe the dominant processes that control TX recombination. In Figure 4, we show the extension of our measurements to TX emission. Figure 4a is a plot of the pulse-integrated third-order correlation. ΔP_{1-2} is

DOI: 10.1021/acs.nanolett.8b02080
Nano Lett. 2018, 18, 5153−5158

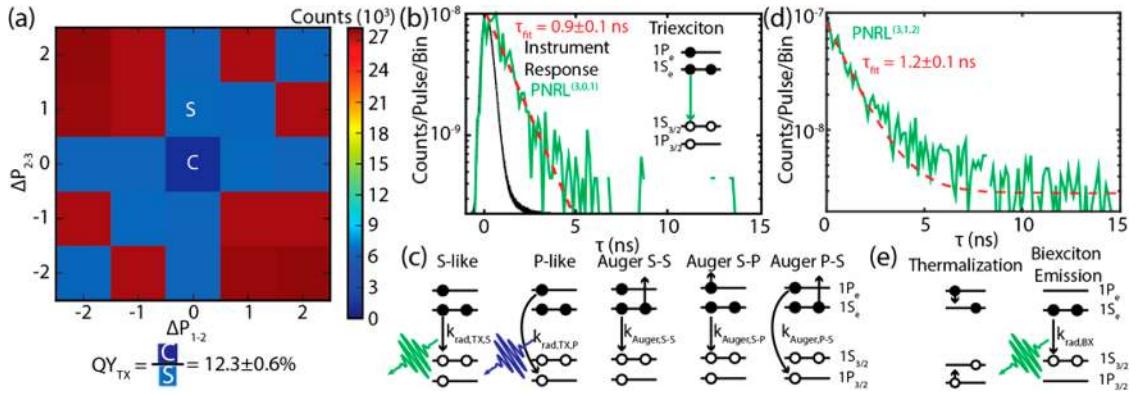

Figure 4. (a) Pulse resolved $g^{(3)}$ experiment. ΔP_{1-2} indicates the pulse difference between photons 1 and 2, and ΔP_{2-3} indicates the pulse difference between photons 2 and 3. The ratio of the counts of the center (C) to side (S) peak is used to calculate the triexciton quantum yield. (b) Triexciton lifetime (green) fit to a single exponential (red). The instrument response is plotted in black for comparison. (c) Possible pathways for triexciton recombination in CdSe NCs, as described in this study. This includes both radiative pathways as well as three Auger pathways. (d) Plot of $PNRL^{(3,1,2)}$ (green) with a fit to an exponential plus a constant (red). (e) Recombination pathway of second photon emission immediately after S-like triexciton emission.

the pulse difference between the first and second photon, and ΔP_{2-3} is the pulse difference between the second and third photon. The analogous positions to the center (C) and side (S) peaks in a second order correlation experiment are marked on the plot. We calculate the TX quantum yield from an extension of the methods described by Nair et al. and Beyler et al. (SI).[10,35]

$$g_0^{(3)} = \frac{G_3}{G_2 G_1} = \frac{QY_{TX}}{QY_X} \tag{3}$$

where $g_0^{(3)}$ is the third-order correlation, G_3 is the area of the center peak (three photons detected after the same laser pulse, Figure 4a, C), and the product of G_2 and G_1 is the area of the side peak (two photons are detected after a single laser pulse and one photon on the subsequent pulse, Figure 4a, S), and QY_{TX}/QY_X is the TX to X quantum yield ratio. We calculate a TX to X quantum yield ratio of 12.3 ± 0.6% for this NC.

We extract the relative increase of the TX radiative lifetime as compared to the X lifetime similarly to how we determine the scaling for the BX in eq 1.

$$r_{TX/X} = \frac{k_{rad,TX}}{k_{rad,X}} = \frac{\tau_X/QY_X}{\tau_{TX}/QY_{TX}} \tag{4}$$

where $r_{TX/X}$ is the relative speed up of the TX radiative rate compared to the X, $k_{rad,TX}$ is the TX radiative rate, $k_{rad,X}$ is the X radiative rate, τ_X is the X lifetime, QY_{TX}/QY_X is the triexciton to exciton quantum yield ratio, and τ_{TX} is the triexciton lifetime. We can predict the value of $r_{TX/X}$ for either S-like or P-like emission. For P-like emission, we utilize Fermi's Golden Rule to predict the radiative rate of the state.[36]

$$k_j \propto \omega_j |\langle i|\mathbf{p}|j\rangle|^2 \tag{5}$$

where k_j is the rate of emission from state j, ω_j is the energy of the state j, and $|\langle i|\mathbf{p}|j\rangle|^2$ is the momentum overlap between states i and j. Since both the S-like and P-like states originate from the same Bloch wave function, the momentum overlap should not differ appreciably.[37] The energy difference between the states in spherical NCs (<250 meV) only causes, at most, a 10% difference in the radiative rate.[20] Additionally, the P-like state has similar fine-structure to the S-like state, resulting in the same factor of 1/2 decrease in the emission rate as compared to a purely emissive state.[22] Therefore, we predict the radiative lifetime of the P-like state to be within 10% of the lifetime of the exciton. For triexciton emission originating from the S-like state, we expect the radiative lifetime to be equivalent to the biexciton radiative lifetime. Thus, $r_{TX/X}$ will be ∼1 for pure P-like emission, $r_{TX/X}$ will be 4 for pure S-like emission, and $r_{TX/X}$ will be ∼5 if both S-like and P-like pathways are active in triexciton recombination. If both pathways are active, emission is dominated by the faster S-like emission.

We extract a speed up of $r_{TX/X}$ = 4.2 ± 0.6 for the triexciton using eq 4 with a triexciton lifetime (Figure 4b) of 0.9 ± 0.1 ns, a triexciton to exciton quantum yield ratio of 12.3%, and an exciton lifetime of 30.5 ns. Since 4.2 falls between the predicted value for pure S-like emission and for both S-like and P-like emission simultaneously, we conclude that triexciton emission dynamics are dominated by S-like recombination.

Although previous studies have demonstrated emission from the P-like state via a spectral shift under high-flux excitation, unlike here, these works have not exclusively isolated triexciton emission from that of higher-order multiexcitons.[19−21] Our analysis above indicates that in order to observe significant P-like emission from a NC, multiexcitons higher than third order are necessary to overcome S-like emission. Indeed, these previous studies had an average of more than two excitons per NC, consistent with this hypothesis.

We next address the nonradiative processes that control the TX quantum yield. We apply the statistical scaling results calculated above to determine the Auger rate for both the biexciton and triexciton. Assuming that the emission rate extracted from the X lifetime is the radiative rate, implying the QY_X is 100%, we can utilize the values measured above and an alternate definition of the biexciton quantum yield to extract Auger rates. From the BX quantum yield, we can extract the BX Auger rate by utilizing the bound BX radiative rate of four times the X radiative rate, or 0.131 ± 0.002 ns^{-1}.

$$QY_{BX} = \frac{k_{rad,BX}}{k_{rad,BX} + k_{nr,BX}} \tag{6}$$

where QY_{BX} is the BX quantum yield, $k_{rad,BX}$ is the BX radiative rate, and $k_{nr,BX}$ is the BX Auger rate. We find the BX Auger rate is 0.77 ± 0.06 ns^{-1} for this NC.

DOI: 10.1021/acs.nanolett.8b02080
Nano Lett. 2018, 18, 5153−5158

$$QY_{TX} = \frac{k_{rad,TX}}{k_{rad,TX} + k_{nr,TX}} \quad (7)$$

where QY_{TX} is the TX quantum yield, $k_{rad,TX}$ is the TX radiative rate, and $k_{nr,TX}$ is the TX Auger rate. The TX Auger rate for this particle is 1.0 ± 0.2 ns^{-1}. Even with multiple new Auger processes between S-like and P-like carriers due to the addition of a third exciton to the system, the total Auger rate is similar for the BX and TX. Thus, the newly added pathways are likely much slower than Auger processes between carriers residing in the band edge S-like state, and the addition of a third exciton does not greatly alter the rate of S-like Auger processes. The similarity in both radiative and Auger rates of the BX and TX account for the similar quantum yields measured for the states.

Measurement of PNRL$^{(3,1,2)}$ (Figure 4d) indicates that the lifetime of the second photon from a TX (1.2 ± 0.1 ns) is equivalent to the BX lifetime (1.1 ± 0.1 ns) measured by PNRL$^{(2,1,2)}$, showing a continued lack of system memory. With the TX emission arising primarily from the S-like state, thermalization must be sufficiently rapid that P-like emission from the newly created hot BX does not occur (Figure 4e). This is consistent with previous experiments studying the thermalization rate in CdSe NCs and by spectrally resolved $g^{(2)}$ measurements showing P-like emission always precedes S-like if P-like emission occurs.[38−41]

In this Letter, we have developed a comprehensive understanding of BX and TX dynamics in CdSe-based NCs of different shell thicknesses under low-flux excitation. First, we have unambiguously demonstrated the often assumed factor of 4 scaling between the X and BX radiative rates for a variety of CdS shell thicknesses, even for thick shell particles with drastically different exchange energies than core only NCs. We utilize our BX results to further show that TX recombination is dominated by both band-edge radiative recombination and Auger processes rather than contributions from the higher-lying P-like state.

■ ASSOCIATED CONTENT

Supporting Information

The Supporting Information is available free of charge on the ACS Publications website at DOI: 10.1021/acs.nanolett.8b02080.

Material characterization, sample preparation, experimental setup, background characterization and subtraction, and $g^{(3)}$ derivation (PDF)

■ AUTHOR INFORMATION

Corresponding Author

*E-mail: mgb@mit.edu. Phone: 617-253-9796.

ORCID

Justin R. Caram: 0000-0001-5126-3829
Hendrik Utzat: 0000-0003-2901-0141
Lea Nienhaus: 0000-0003-1412-412X
Moungi G. Bawendi: 0000-0003-2220-4365

Present Address

†Department of Chemistry and Biochemistry, University of California, Los Angeles, 607 Charles E Young Drive, Los Angeles, California 90095, United States.

Author Contributions

‡These authors contributed equally. The manuscript was written through contributions of all authors. All authors have given approval to the final version of the manuscript.

Notes

The authors declare no competing financial interest.

■ ACKNOWLEDGMENTS

This work was supported primarily by the Center for Excitonics, an Energy Frontier Research Center funded by the U.S. Department of Energy, Office of Science, Basic Energy Sciences under Award No. DE-SC0001088. K.E.S. (lead author, data collection, analysis and interpretation, software development), T.S.B. (study conception, data collection, analysis and interpretation), and L.N. (sample characterization) were supported through the Center for Excitonics. H.U. (analysis software development) and J.R.C. (data interpretation) were supported by the United States Department of Energy, Office of Basic Energy Sciences, Division of Materials Sciences and Engineering (Award No. DE-FG02-07ER46454). I.C. (CdSe/CdS shell-series synthesis) was supported by the National Science Foundation Graduate Research Fellowship.

■ ABBREVIATIONS

NC, nanocrystal; PL, photoluminescence; PNRL, photon number resolved lifetime; X, exciton; BX, biexciton; TX, triexciton; QY, quantum yield

■ REFERENCES

(1) Wood, V.; Bulović, V. *Nano Rev.* **2010**, *1*, 5202.
(2) Dang, C.; Lee, J.; Breen, C.; Steckel, J. S.; Coe-Sullivan, S.; Nurmikko, A. *Nat. Nanotechnol.* **2012**, *7*, 335−339.
(3) Mashford, B. S.; Stevenson, M.; Popovic, Z.; Hamilton, C.; Zhou, Z.; Breen, C.; Steckel, J.; Bulovic, V.; Bawendi, M.; Coe-Sullivan, S.; et al. *Nat. Photonics* **2013**, *7*, 407−412.
(4) Anikeeva, P. O.; Halpert, J. E.; Bawendi, M. G.; Bulović, V. *Nano Lett.* **2009**, *9*, 2532−2536.
(5) Klimov, V. I.; Mikhailovsky, A. A.; Xu, S.; Malko, A.; Hollingsworth, J. A.; Leatherdale, C. A.; Eisler, H.-J.; Bawendi, M. G. *Science* **2000**, *290*, 314−317.
(6) Brokmann, X.; Giacobino, E.; Dahan, M.; Hermier, J. P. *Appl. Phys. Lett.* **2004**, *85*, 712−714.
(7) Bawendi, M. G.; Steigerwald, M. L.; Brus, L. E. *Annu. Rev. Phys. Chem.* **1990**, *41*, 477−496.
(8) Chen, O.; Zhao, J.; Chauhan, V. P.; Cui, J.; Wong, C.; Harris, D. K.; Wei, H.; Han, H.-S.; Fukumura, D.; Jain, R. K.; et al. *Nat. Mater.* **2013**, *12*, 445−451.
(9) Bae, W. K.; Padilha, L. A.; Park, Y.; McDaniel, H.; Robel, I.; Pietryga, J. M.; Klimov, V. I. *ACS Nano* **2013**, *7*, 3411−3419.
(10) Beyler, A. P.; Bischof, T. S.; Cui, J.; Coropceanu, I.; Harris, D. K.; Bawendi, M. G. *Nano Lett.* **2014**, *14*, 6792−6798.
(11) Bischof, T. S.; Caram, J. R.; Beyler, A. P.; Bawendi, M. G. *Opt. Lett.* **2016**, *41*, 4823−4826.
(12) García-Santamaría, F.; Brovelli, S.; Viswanatha, R.; Hollingsworth, J. A.; Htoon, H.; Crooker, S. A.; Klimov, V. I. *Nano Lett.* **2011**, *11*, 687−693.
(13) Nasilowski, M.; Spinicelli, P.; Patriarche, G.; Dubertret, B. *Nano Lett.* **2015**, *15*, 3953−3958.
(14) Kong, D.; Jia, Y.; Ren, Y.; Xie, Z.; Wu, K.; Lian, T. *J. Phys. Chem. C* **2018**, *122*, 14091.
(15) Klimov, V. I.; Mikhailovsky, A. A.; McBranch, D. W.; Leatherdale, C. A.; Bawendi, M. G. *Science* **2000**, *287*, 1011−1013.
(16) Califano, M.; Franceschetti, A.; Zunger, A. *Phys. Rev. B: Condens. Matter Mater. Phys.* **2007**, *75*, 1−12.

DOI: 10.1021/acs.nanolett.8b02080
Nano Lett. 2018, 18, 5153−5158

(17) Canneson, D.; Biadala, L.; Buil, S.; Quelin, X.; Javaux, C.; Dubertret, B.; Hermier, J. P. *Phys. Rev. B: Condens. Matter Mater. Phys.* **2014**, *89*, 1−5.
(18) Klimov, V. I.; McGuire, J. A.; Schaller, R. D.; Rupasov, V. I. *Phys. Rev. B: Condens. Matter Mater. Phys.* **2008**, *77*, 1−12.
(19) Caruge, J. M.; Chan, Y.; Sundar, V.; Eisler, H. J.; Bawendi, M. G. *Phys. Rev. B: Condens. Matter Mater. Phys.* **2004**, *70*, 1−7.
(20) Fisher, B.; Caruge, J. M.; Chan, Y. T.; Halpert, J.; Bawendi, M. G. *Chem. Phys.* **2005**, *318*, 71−81.
(21) Fisher, B.; Caruge, J. M.; Zehnder, D.; Bawendi, M. *Phys. Rev. Lett.* **2005**, *94*, 1−4.
(22) Franceschetti, A.; Troparevsky, M. C. *J. Phys. Chem. C* **2007**, *111*, 6154−6157.
(23) Osovsky, R.; Cheskis, D.; Kloper, V.; Sashchiuk, A.; Kroner, M.; Lifshitz, E. *Phys. Rev. Lett.* **2009**, *102*, 1−4.
(24) Oron, D.; Kazes, M.; Shweky, I.; Banin, U. *Phys. Rev. B: Condens. Matter Mater. Phys.* **2006**, *74*, 1−6.
(25) Zhao, J.; Chen, O.; Strasfeld, D. B.; Bawendi, M. G. *Nano Lett.* **2012**, *12*, 4477−4483.
(26) Canneson, D.; Mallek-Zouari, I.; Buil, S.; Quélin, X.; Javaux, C.; Dubertret, B.; Hermier, J. P. *New J. Phys.* **2012**, *14*, 1−16.
(27) Coropceanu, I.; Bawendi, M. G. *Nano Lett.* **2014**, *14*, 4097−4101.
(28) Fisher, B. R.; Eisler, H.-J.; Stott, N. E.; Bawendi, M. G. *J. Phys. Chem. B* **2004**, *108*, 143−148.
(29) van Driel, A. F.; Allan, G.; Delerue, C.; Lodahl, P.; Vos, W. L.; Vanmaekelbergh, D. *Phys. Rev. Lett.* **2005**, *95*, 236804.
(30) Chamarro, M.; Gourdon, C.; Lavallard, P.; Lublinskaya, O.; Ekimov, A. I. *Phys. Rev. B: Condens. Matter Mater. Phys.* **1996**, *53*, 1336−1342.
(31) Efros, A.; Rosen, M.; Kuno, M.; Nirmal, M.; Norris, D.; Bawendi, M. *Phys. Rev. B: Condens. Matter Mater. Phys.* **1996**, *54*, 4843−4856.
(32) Accanto, N.; Masia, F.; Moreels, I.; Hens, Z.; Langbein, W. *ACS Nano* **2012**, *6*, 5227−5233.
(33) Moreels, I.; Raino, G.; Gomes, R.; Hens, Z.; Stoferle, T.; Mahrt, R. F. *ACS Nano* **2011**, *5*, 8033−8039.
(34) Shabaev, A.; Rodina, A. V.; Efros, A. L. *Phys. Rev. B: Condens. Matter Mater. Phys.* **2012**, *86*, 1−14.
(35) Nair, G.; Zhao, J.; Bawendi, M. G. *Nano Lett.* **2011**, *11*, 1136−1140.
(36) van Driel, A. F.; Allan, G.; Delerue, C.; Lodahl, P.; Vos, W. L.; Vanmaekelbergh, D. *Phys. Rev. Lett.* **2005**, *95*, 1−4.
(37) Efros, Al. L.; Rosen, M. *Annu. Rev. Mater. Sci.* **2000**, *30*, 475−521.
(38) Hendry, E.; Koeberg, M.; Wang, F.; Zhang, H.; de Mello Donegá, C.; Vanmaekelbergh, D.; Bonn, M. *Phys. Rev. Lett.* **2006**, *96*, 1−4.
(39) Klimov, V. I.; McBranch, D. W.; Leatherdale, C. A.; Bawendi, M. G. *Phys. Rev. B: Condens. Matter Mater. Phys.* **1999**, *60*, 13740−13749.
(40) Klimov, V. I. *J. Phys. Chem. B* **2000**, *104*, 6112−6123.
(41) Kambhampati, P. *Acc. Chem. Res.* **2011**, *44*, 1−13.

DOI: 10.1021/acs.nanolett.8b02080
Nano Lett. 2018, 18, 5153−5158